Neuron
Article

Feedforward Origins of Response Variability Underlying Contrast Invariant Orientation Tuning in Cat Visual Cortex

Srivatsun Sadagopan[1,2] and David Ferster[1,*]
[1]Department of Neurobiology, Northwestern University, 2205 Tech Drive, Evanston, IL 60208, USA
[2]Present address: Laboratory of Neural Systems, The Rockefeller University, 1230 York Avenue, New York, NY 10065, USA
*Correspondence: ferster@northwestern.edu
DOI 10.1016/j.neuron.2012.05.007

SUMMARY

Contrast invariant orientation tuning in simple cells of the visual cortex depends critically on contrast dependent trial-to-trial variability in their membrane potential responses. This observation raises the question of whether this variability originates from within the cortical circuit or the feedforward inputs from the lateral geniculate nucleus (LGN). To distinguish between these two sources of variability, we first measured membrane potential responses while inactivating the surrounding cortex, and found that response variability was nearly unaffected. We then studied variability in the LGN, including contrast dependence, and the trial-to-trial correlation in responses between nearby neurons. Variability decreased significantly with contrast, whereas correlation changed little. When these experimentally measured parameters of variability were applied to a feedforward model of simple cells that included realistic mechanisms of synaptic integration, contrast-dependent, orientation independent variability emerged in the membrane potential responses. Analogous mechanisms might contribute to the stimulus dependence and propagation of variability throughout the neocortex.

INTRODUCTION

When Hubel and Wiesel (1962) first described orientation selectivity in the cat visual cortex, they proposed a simple and powerful model for how it might arise. In their model, the aggregate synaptic input to cortical simple cells derives its orientation selectivity from the alignment of the receptive fields of the presynaptic thalamic relay cells. In its simplest form, however, this basic model failed to explain several features of sensory responses subsequently observed in quantitative studies of simple cell behavior (Priebe and Ferster, 2008), including the sharpness of orientation tuning, cross-orientation suppression, and—of interest in the present study—contrast-invariant orientation tuning (Sclar and Freeman, 1982; Skottun et al., 1987; Alitto and Usrey, 2004). By definition, contrast invariance requires that the width of orientation tuning remain constant in the face of changing stimulus strength (contrast). Constant tuning width, in turn, requires that low-contrast stimuli in the optimal orientation evoke higher numbers of spikes than do high-contrast orthogonal stimuli. And yet, it has been shown in previous studies that both these stimuli evoke nearly identical mean depolarizations (Finn et al., 2007), as predicted on theoretical grounds from the lack of orientation tuning in thalamic inputs (Ferster and Miller, 2000).

Finn et al. (2007) explained this apparent paradox by showing that the amplitude of the responses to low-contrast stimuli varied more from trial to trial than did the responses to high-contrast stimuli. Even though two stimuli, one low contrast and one high contrast, might evoke the same mean depolarization, the higher variability gave the low-contrast stimulus a much higher probability of pushing the membrane potential (V_m) above threshold on some trials. Thus, trial-to-trial variability and its contrast dependence are crucial to establishing the precise pattern of visual responses in simple cells that is missing from the simplest versions of the feedforward model.

While trial-to-trial variability in V_m responses can explain the origins of contrast invariant tuning, it raises the next logical question of where the variability itself originates. Two possibilities immediately present themselves. The first is that variability is generated de novo and is modulated in a stimulus specific manner within the cortical circuit. Variability could be modulated, for example, by shunting inhibition (Borg-Graham et al., 1998; Sit et al., 2009) or generated by chaotic behavior in feedback connections (Rajan et al., 2010). The second possibility is that sufficient variability is present in the thalamic inputs to the cortex and is propagated directly to simple cells. In this study, we address these two possibilities in turn. We first show that inactivating the surrounding cortex has little effect on response variability in the V_m responses of simple cells, suggesting that variability originates from feedforward thalamic inputs. We then show that response variability in the lateral geniculate nucleus (LGN) is contrast dependent and is correlated between cells. When these two features of the thalamic input are incorporated into an experimentally constrained feedforward model, contrast dependence of variability in the V_m responses of simple cells emerges, and matches the variability observed in vivo. Thus, we can now provide a mechanistic account of how variability arises in V1 and how it gives rise to contrast-invariant orientation tuning. Stimulus-dependent changes in variability

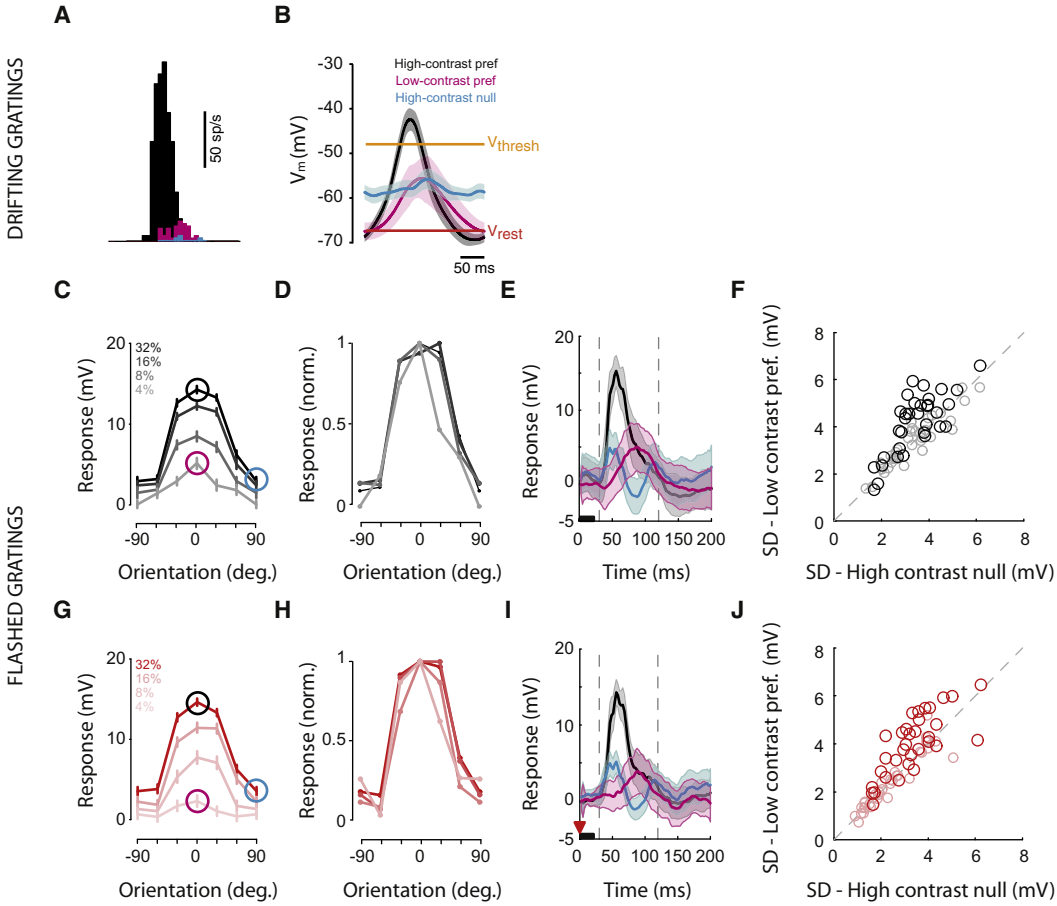

Figure 1. Contrast Dependence of Simple Cell V_m Variability in Intact and Inactivated Cortex

(A) PSTHs of spike responses recorded from a simple cell in response to high-contrast preferred (black), high-contrast null (cyan), and low-contrast preferred (magenta) drifting gratings.

(B) Mean V_m (solid lines) for one cycle of the response to drifting gratings (same cell as in A). Shading is cycle-to-cycle V_m SD. Red and orange lines are resting membrane potential and approximate spike threshold. Note that threshold is near the peak of the response to optimal orientation and contrast. (A) and (B) are adapted from Finn et al., 2007.

(C) Orientation tuning curves of an example simple cell responding to flashed gratings at 4 stimulus contrasts (4%, 8%, 16% and 32%) in the intact cortex. Circles indicate the high-contrast preferred (black), high-contrast null (cyan), and low-contrast preferred (magenta) responses. Error bars correspond to SEM.

(D) Same as (C), but normalized to maximum response level at each contrast.

(E) V_m means (lines) and V_m SDs (shading) of this simple cell's responses to high-contrast preferred (black), high-contrast null (cyan), and low-contrast preferred (magenta) flashed gratings. Black bar corresponds to stimulus duration. Dashed lines represent the analysis window within which the peak response was detected (30–120 ms after stimulus onset).

(F) The trial-to-trial V_m SD of peak responses for low-contrast preferred gratings plotted against the V_m SD of high-contrast null gratings (n = 35 simple cells), measured at the peak of the response (black circles), and during the baseline period (gray circles).

(G–J) Same as (C)–(F) but after cortical inactivation by local electrical stimulation delivered at the start of the visual stimulus (red arrow). Red circles and light red circles in (H) correspond to peak V_m SD during the stimulus-evoked response period and baseline period (between 5 and 10 ms following stimulus onset).

See also Figures S2 and S3.

are a widespread phenomenon, and have been observed throughout the neocortex (Churchland et al., 2010). Principles similar to the ones discussed here may contribute to the generation and propagation of variability in these areas as well.

RESULTS

A fundamental requirement for contrast invariant orientation tuning is that low-contrast gratings at the preferred orientation evoke more spikes than do high-contrast gratings at the non-preferred orientation. This relationship is observed in the spiking responses of V1 simple cells (Figure 1A). Yet, the peak depolarizations of the underlying V_m evoked by these two stimuli are—when averaged over multiple stimulus cycles—very similar (Figure 1B, magenta and cyan traces). This relationship highlights one of the central puzzles presented by contrast-invariant orientation tuning in V1—how two stimuli that evoke the same mean depolarization evoke very different numbers of spikes.

Finn et al. (2007) resolved this apparent paradox by taking into account the trial-to-trial variability of visually evoked depolarizations. Though the mean depolarization evoked by one cycle of a low-contrast preferred grating and high-contrast null grating were both well below threshold, the low-contrast preferred response had far greater trial-to-trial variability, as measured by the standard deviation (SD) of response amplitude (Figure 1B, shading). This increase in variability, in turn, increased the likelihood that V_m crossed threshold and evoked spikes on any given trial. Note that although variability decreased with contrast, it depended little on either stimulus orientation, or response amplitude. Here, we test two possible sources of contrast dependent changes in variability: 1) the local cortical circuit and 2) feedforward thalamocortical projections.

Contrast Dependence of Simple Cell V_m Variability during Cortical Inactivation

We first test—using a loss-of-function approach—whether the high variability observed at low stimulus contrasts is generated locally. If the cortical circuit contributes to response variability, for example, through its recurrent elements, then silencing the cortex should reduce that variability. To silence a small patch of the cortex around the recording electrode, we used local electrical stimulation (Chung and Ferster, 1998) and compared trial-to-trial variability before and during inactivation. Since electrical stimulation only affords a brief (~100 ms) period during which the cortex is silenced, we measured variability and the effects of cortical silencing in the responses to briefly flashed gratings instead of drifting gratings.

Before inactivating the cortex, we first examined whether orientation tuning of the V_m responses to flashed gratings was, in fact, contrast-invariant, as it is for drifting gratings. For the example cell in Figure 1, the width of orientation tuning was indeed similar across contrasts (Figure 1C), with only a slight narrowing at the lowest contrast (4%), as can be seen in the normalized tuning curves of Figure 1D. Over the population, tuning width at high contrast (mean $\sigma = 32^\circ$) was not significantly different than it was at low contrast (35°; paired t test, $p = 0.20$; $n = 21$).

We next confirmed that the trial-to-trial variability in V_m responses increases with decreasing contrast for flashed gratings as it does for drifting gratings. This change in variability can be seen in Figure 1E by comparing the trial-to-trial SD of the responses at high-contrast (gray and cyan shading) with the low-contrast SD (magenta shading). Detailed changes in the distribution of the response amplitudes in four additional cells are shown as kernel density estimates in Figure S2A (available online), where it can be seen that the V_m distributions evoked by low-contrast preferred stimuli were wider or more right-skewed than those evoked by high-contrast null stimuli. An indication of the contrast-dependent, but orientation-independent changes in variability can also be seen in the error bars (SEM) of Figure 1C (compare circles).

We quantified peak V_m variability for each stimulus condition as the SD of the V_m response in a 2.5 ms window centered on the peak of the mean V_m response. For the population of cells in Figure 1, the peak V_m SDs for high-contrast preferred stimuli, high-contrast null stimuli and low-contrast preferred stimuli were 3.66, 3.24, and 3.88 mV, similar to the values observed for drifting grating stimuli. Of the 35 cells studied, 26 showed higher V_m variability for low-contrast preferred stimuli (~75%) than for high-contrast null stimuli. On average, peak V_m variability for low-contrast preferred stimuli was 22% greater than variability for high-contrast null stimuli ($n = 35$, $p < 0.01$, paired t test; Figure 1F). Thus, the signature criterion for contrast-invariance, that low-contrast preferred V_m responses are more variable than high-contrast null responses, was met for flashed gratings as well as for drifting gratings.

We next recorded the responses to flashed gratings with the cortex inactivated. We silenced local cortical activity with a single electrical shock (300–400 μA, 200 μs, electrode negative) delivered through a low-impedance metal electrode placed in the upper layers of the cortex, typically within 500 μm of the patch pipette. This configuration has been shown to silence spiking for 50 ms in a 1–2 mm diameter region of cortex, while having little effect on visual responses in the LGN (Chung and Ferster, 1998). During inactivation, the cell in Figure 1 showed only a 10% decrease in its response to high-contrast preferred gratings, suggesting that the thalamus contributed a large fraction of the excitatory inputs. Orientation tuning remained largely contrast invariant in that the width of tuning was similar at all contrasts (Figures 1G and 1H). As in the intact cortex, during inactivation, tuning widths at high and low contrasts were similar across the population (mean σ 32° and 36°; paired t test, $p = 0.12$). And as observed previously (Chung and Ferster, 1998), the width of orientation tuning at each contrast was minimally changed by the cortical inactivation (compare Figure 1C and G; paired t test, $p = 0.69$ at 32%, $p = 0.92$ at 4%).

Just prior to the response onset (0–30 ms), the shock caused a clear reduction in V_m variability. This reduction is visible when comparing the width of shading (SD) with and without shock (compare Figures 1E and 1I just after the start of the traces; summarized in Figure 2A). Once the visually evoked response began, however, variability in all cases returned to a level comparable to the flash-only condition (compare shading in Figures 1E and 1I at response peaks; summarized in Figure 2B). Kernel density estimates of the V_m distributions of four additional simple cells during cortical inactivation also showed increased V_m variability for low-contrast preferred gratings (Figure S2B). During inactivation, 25 out of 35 cells (~72%) showed higher V_m variability for low-contrast preferred stimulation. Of the 26 neurons that originally showed higher V_m variability for low contrast preferred stimuli in the intact cortex, 21 cells (80%) retained higher V_m variability after cortical inactivation. On average, V_m variability for low-contrast preferred stimuli was 20% greater than variability for high-contrast null stimuli (Figure 1J; $p < 0.01$, paired t test), compared to 22% for the intact cortex.

The effects of inactivation on the SD ratio (low-contrast preferred/high-contrast null) are shown for individual neurons in Figure 2C, where the SD ratio for inactivated cortex is plotted against the SD ratio for intact cortex. The plot shows considerable scatter, as some cells show greater SD at high contrast than at low contrast in the intact cortex (upper left quadrant) and others show a greater SD at high contrast than at low contrast during inactivation (lower right quadrant). For these

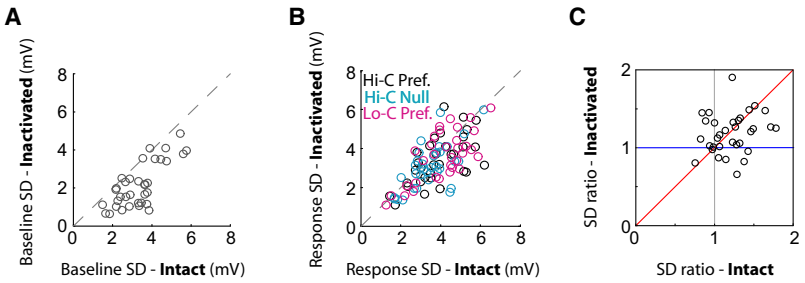

Figure 2. Contribution of Cortical Activity to Stimulus-Evoked V_m Variability

(A) Baseline V_m SD of responses pooled across all stimulus conditions in inactivated cortex plotted against pooled baseline V_m SD in intact cortex.

(B) V_m SD during the stimulus-evoked response period in inactivated cortex plotted against response V_m SD in intact cortex for high-contrast preferred (black), high-contrast null (cyan) and low-contrast preferred (magenta) stimuli.

(C) The percent increase in V_m SD for low-contrast preferred stimuli compared to high-contrast null stimuli after cortical inactivation plotted against the same measure in intact cortex. Red line, the prediction from a thalamic-origin model of variability; blue line, the prediction from a cortical-origin model.

cells, cortical inactivation suppressed the SD ratio. But the upper right quadrant—where low-contrast SD is greater than high-contrast SD—is the most populated, and many of the cells in this quadrant lie along the diagonal; their SD ratios changed little during inactivation.

To evaluate the overall trend in the plot of Figure 2C, we can compare these data to what the two models for the origin of contrast dependent variability might predict. A thalamic origin predicts that cortical inactivation would have no effect on the SD ratio: the SD ratio would be identical for intact and inactivated cortex, and all of the points would lie along the diagonal (red). A cortical origin predicts that cortical inactivation would abolish much of the difference in variability between low and high contrast. The SD ratio would therefore be reduced toward 1, and the points would lie along a horizontal line at 1 (blue). We can test these two predictions statistically. Since the fit to the points in Figure 2C is not significantly different from the diagonal ($p = 0.71$, paired t test) but was significantly different from a horizontal line at a value of 1 ($p < 0.001$), the data favor a thalamic origin for contrast-dependent changes in response variability.

In addition to the control experiments of Chung and Ferster (1998), five observations confirmed that the electrical stimulus was effective in inactivating the cortex. First, mean spiking activity (pooled across all trials) was reduced more than 40-fold to 0.007 spike/trial, and peak spike rates were reduced 30-fold after cortical inactivation. Second, mean V_m responses to high-contrast preferred gratings were smaller after inactivation (52% reduction on average, $n = 35$), likely from the suppression of intracortical activity. Third, a marked hyperpolarization of V_m was evident immediately following the shock artifact, suggesting that the shock evoked a large inhibitory potential, which is likely one of the mechanisms by which spiking activity is silenced. Fourth, as noted above, V_m variability immediately following the shock, but before the visual response, was markedly lower than the resting variability. In the time window between 5–10 ms following the shock, the trial-to-trial SD of the membrane potential was reduced relative to the resting cortex by 39% ($p < 0.01$, paired t test), pooled across all stimulus types (Figure 2B). Fifth, as observed previously (Finn et al., 2007), the fraction of thalamic inputs to these simple cells was highly correlated to their DC-Null/DC-Pref ratios (Figure S3B). Here, DC-Null and DC-Pref are the mean depolarizations evoked by high-contrast gratings at the null and preferred orientations. Because LGN responses are themselves not tuned to orientation, this ratio for the LGN input to a simple cell should be 1. Conversely, because the spike responses of cortical cells are orientation specific, this ratio for cortical inputs to a simple cell should be 0. Cells are therefore predicted to have a DC-Null/DC-Pref ratio in proportion to the excitatory input that originates in the LGN, and the correlation observed in Figure S3B becomes an indication of the effectiveness of the inactivation.

Overall, then, cortical inactivation resulted in lower response means and lower baseline variability, but critically, stimulus-evoked V_m variability was spared (Figure 2B). For the three stimulus conditions indicated, V_m variability was on average ~10% lower after cortical shock compared to the variability in intact cortex, but this difference was not statistically significant. These data strongly suggest that the stimulus-evoked V_m variability observed in simple cells is not caused by local cortical activity. Given that these cells receive, on average, about half of their inputs from the thalamus, it is likely that a large proportion of visually evoked V_m variability originates in feedforward activity from the LGN.

Contrast Dependence of Spike Count Variability in LGN Neurons

The shock experiments suggest that variability and its dependence on contrast does not require an intact cortical circuit but might instead be inherited from the LGN, through the same feedforward circuit that establishes orientation selectivity. To test this possibility, we measured variability in the responses of LGN cells, applied that variability to a simple feedforward model, and asked whether—and under what assumptions—the behavior of the model matches the behavior of the V_m responses of simple cells.

This problem requires more than merely recording the variability in single LGN cells, however. Even if LGN responses were highly variable, if the variability were uncorrelated among individual LGN cells, the variability would be washed out in the membrane potential of a downstream simple cell because of pooling, or averaging of inputs. This reduction of variability would be largely mitigated, however, if the trial-to-trial variability were correlated between nearby LGN cells. Therefore, in addition to measuring contrast-dependent variability in single LGN cells, we also measured the correlation in trial-to-trial variability within groups of LGN neurons with close or overlapping receptive fields (center-to-center distance < 2.5°).

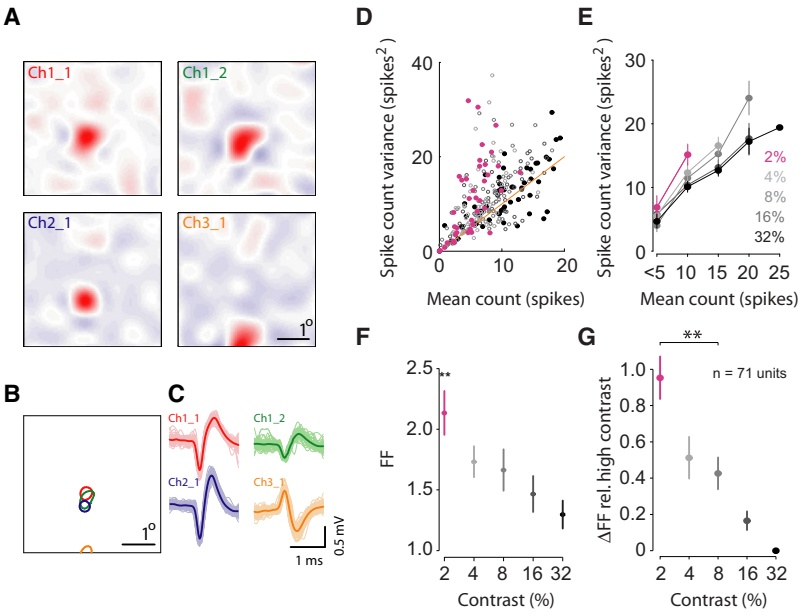

Figure 3. Contrast Dependence of Spike Count Variability in the LGN

(A) Receptive field maps constructed from sparse noise stimuli for four ON-center LGN neurons recorded simultaneously on three different electrodes.

(B) The 80% extent of the receptive fields of the above neurons overlaid.

(C) Randomly chosen spike waveforms (thin lines) and mean waveforms (thick lines) of the four neurons in (A) and (B).

(D) Trial-to-trial variance of the spike count (calculated from the positive half-cycle of the response) plotted against the mean spike count for 5 contrasts in 71 LGN neurons. Orange line is the Poisson expectation (variance = mean).

(E) Trial-to-trial variance of spike count averaged across neurons with mean spike counts in 5 different ranges (0–5, 5–10, 10–15, etc.), for each different contrast. Colors as in (D). Error bars as ± 1 SEM.

(F) The population means of Fano factor (FF) plotted as a function of contrast.

(G) The population means of the change in Fano factor (FF) relative to 32% contrast plotted as a function of contrast. ** denotes $p < 0.01$, multiple-comparison corrected ANOVA. Error bars correspond to SEM (n = 71 LGN cells).

See also Figure S4.

In Figure 3, four ON-center neurons were recorded simultaneously on three electrodes. Individual receptive field maps (Figure 3A), and superimposed receptive field contours at 80% of the maximum response (Figure 3B) show three of the receptive fields to be overlapping, with the fourth just over 1° distant. Spike waveforms of the two cells recorded on the same electrode were easily distinguished (Figure 3C, red and green). Spike rasters and cycle-averaged histograms of the responses at different orientations and contrasts are shown in Figure S4.

For each recorded cell we pooled spike counts across orientation, calculated the mean rate and variance in the positive half-cycle at 5 different contrasts, and plotted variance against mean spike count in Figure 3D. At the highest contrast (32%, black), spike count variance was 20% larger than the mean spike count (Fano factor = 1.2), which is slightly more than expected from a Poisson process (orange line: Fano factor = 1). As the stimulus contrast decreased, LGN responses deviated even more from the Poisson expectation, with Fano factors of 1.46, 1.66, 1.72, and 2.08 at 16%, 8%, 4%, and 2% contrast (Figure 3F), consistent with earlier studies (Sestokas and Lehmkuhle, 1988; Hartveit and Heggelund, 1994).

Over the population (n = 71), we found that the average Fano factor (FF) at low contrast (Figure 3F, magenta) was significantly higher than at the highest contrast tested (Figure 3F, black) ($p < 0.01$, multiple-comparison corrected ANOVA). We also computed the contrast-dependent changes in FF of individual units relative to their FFs at the highest contrast (Figure 3G): The Fano factor at 2% and 4% was 96% and 51% higher than at 32% contrast ($p < 0.01$, multiple-comparison corrected ANOVA). It is important to note that the differences in variability between low and high contrast were related to the stimulus contrast itself and not to the contrast-dependent differences in response amplitude: when we compared variability in subsets of responses with matched spike counts, variability at low contrast was higher than at high contrast. For example, if we selected only those points in Figure 3D for which the mean spike counts lay between 5 and 10 spikes per trial, the variability for low-contrast stimuli had much higher spike count variance than high-contrast stimuli (~15 spikes^2 versus ~9 spikes^2). The same was true for all bins of 5 spikes/trial in width (Figure 3E).

Contrast Dependence of Spike Count Correlations in LGN Neurons

Although trial-to-trial variability in LGN activity depends on contrast, this variability will not propagate to the membrane potential of simple cells unless it is correlated among the presynaptic LGN neurons (see above). To measure response correlations, we recorded simultaneously from pairs of LGN neurons whose receptive field centers lay within 2.5° of one another, under the assumption that only nearby LGN cells would be likely to synapse onto the same simple cell. We then plotted the z-scores of the single-trial spike counts from one neuron against those of a second neuron (Figure 4A). Pairwise correlations emerge as an elongation in the cloud of points and can be quantified with the Pearson correlation coefficient (Experimental Procedures). For the example pairs in Figure 4A, noise correlation changed little with contrast (0.135 at 32% and 0.204 at 4%). Across cells (n = 123), pairwise correlation ranged between 0.1 and 0.15, and did not show any trend with changing contrast (Figure 4B, black). Likewise, no significant relationship between correlation and stimulus contrast was observed when each pair's correlations at lower contrasts were expressed relative to that pair's correlation at 32% contrast (Figure 4C).

The correlation in variability between two cells depended on whether or not they were excited in-phase by the drifting grating stimuli. We separately computed pairwise correlations using stimulus orientations that were aligned to and orthogonal to the axis connecting the two receptive field centers (Figure 4B,

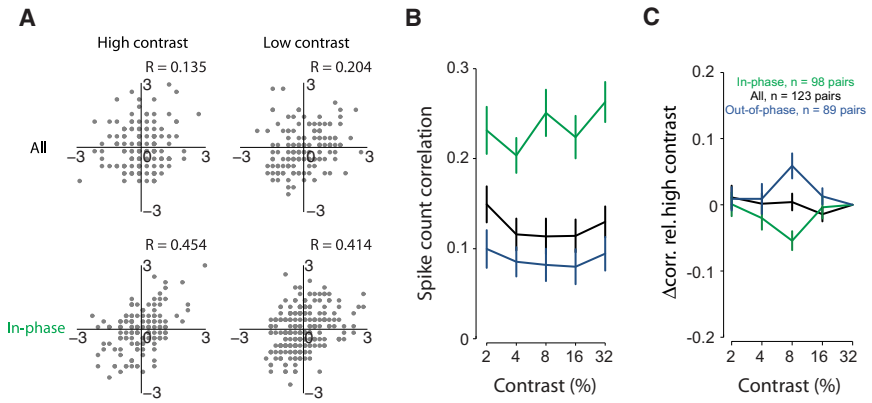

Figure 4. Contrast Independence of Pairwise Correlations between LGN Neurons

(A) Plots of trial-to-trial covariations of spike count for representative pairs of LGN neurons at high and low contrasts, for all responses and in-phase responses. Z-scores of the trial-to-trial spike counts of neuron pairs (gray dots) are plotted against each other. R values are Pearson correlation coefficients.

(B) Pairwise spike count correlations (computed during the positive half-cycle of the response) averaged across the full population of recorded pairs of LGN neurons plotted as a function of contrast. Correlations were calculated over all responses (black), only in-phase LGN responses (green) and out-of-phase LGN responses (blue).

(C) The difference in pairwise correlation between LGN neurons at various contrasts relative to the correlation at high contrast for all responses (black), in-phase responses (green) and out-of-phase responses (blue). Error bars correspond to SEM.

See also Figure S4.

green and blue). In the aligned case, the two LGN cells responded in-phase (>70% overlap in total PSTH area), whereas in the orthogonal, the cells responded out-of-phase (<30% overlap of total PSTH area). Correlations for aligned stimuli were more than twice those for orthogonal stimuli. For neither type of stimulus, however, did pairwise correlations change significantly with contrast (example pair in Figure 4A, bottom; population averages in Figure 4B).

For comparison with the V1 inactivation experiments in which we presented flashed gratings, we also measured variability and cell-to-cell correlation in the responses of LGN neurons to flashed gratings. The results were similar to those derived from drifting gratings. Spike count variability in a 100 ms window starting 30 ms after stimulus onset was higher at low contrasts than at high contrasts (n = 26 cells; FF at 4% = 1.51, FF at 32% = 0.96; $p < 0.01$, multiple-comparison corrected ANOVA). Cell-to-cell correlation was 0.31 (Pearson correlation coefficient; n = 19 pairs; 117–1,170 trials in which PSTHs overlapped by at least 60%; all-way shuffle corrected). Note that to obtain sufficient numbers of stimulus trials for these measurements, data were pooled across orientation and contrast. That is, we assumed—by analogy to the data from drifting gratings—that correlations for flash-evoked responses depend on neither of these parameters.

Contrast-Dependent V_m Variability in a Feedforward Model of Cortical Simple Cells

We next applied the measurements of LGN response variability and its correlation between cells to a feedforward model of cortical simple cells. If the model could account for the contrast-dependent variability in the V_m responses of simple cells, then, from Finn et al. (2007) it could also provide a mechanism for contrast invariance of orientation tuning in simple cells. The receptive field of each modeled simple cell consisted of two adjacent subfields, one ON and one OFF. Each subfield was constructed from multiple LGN inputs, the receptive fields of which were evenly distributed along the preferred orientation axis (Figure 5A). The number of LGN inputs per subfield was initially set to 8, and the subfield aspect ratio set to 3 (Kara et al., 2002). The response properties of the constituent LGN neurons, specifically the mean response rate at each contrast, trial-to-trial variability, and pairwise correlation in response, were drawn, with resampling permitted, from the recorded population of LGN cells (Experimental Procedures). For each iteration of the model, we generated 16 different input neurons based on the LGN data set and simulated their responses to 100 cycles of a drifting grating presented at varying orientations and contrasts. LGN response PSTHs were simulated as half-wave rectified sinusoids (Figure 5A, red and blue traces are average PSTHs of LGN ON and OFF cells). The amplitude of the sinusoid for each LGN cell in a given stimulus cycle was varied in accord with its own trial-to-trial variability and with the pairwise correlation of its variability with other LGN cells in the model. Pairwise correlations between LGN input neurons were generated according to Equation 3 and Equation 4 (Experimental Procedures).

Each presynaptic LGN cell generated a change in conductance in the postsynaptic simple cell in proportion to its firing rate. In other words, the total stimulus-evoked change in conductance in the simple cell (Δg_{exc}) was taken to be proportional to the total spike rate in the presynaptic simple cells. The visually-evoked depolarization in the simple cell then becomes

$$\Delta V_m = \frac{\Delta g_{exc} E_{exc} + g_{rest} E_{rest}}{g_{exc} + g_{rest}} \qquad \text{(Equation 1)}$$

where g_{rest} is the resting or leak conductance of the cell, and E_{rest} it's reversal potential. Dividing through by g_{rest} and expressing all potentials relative to E_{rest}, this can be rewritten as

$$\Delta V_m = \frac{\frac{\Delta g_{exc}}{g_{rest}} E'_{exc}}{1 + \frac{\Delta g_{exc}}{g_{rest}}} \qquad \text{(Equation 2)}$$

where E'_{exc} is the excitatory reversal potential relative to E_{rest}. The scale factor between total LGN spike rate and $\Delta g_{exc}/g_{rest}$ was set such that high-contrast, optimally oriented stimuli evoked an average peak depolarization of 20 mV in the simple cell (Finn et al., 2007). For example, for a simple cell with an input resistance of 80 MΩ (g_{rest} = 12 nS), high contrast gratings would

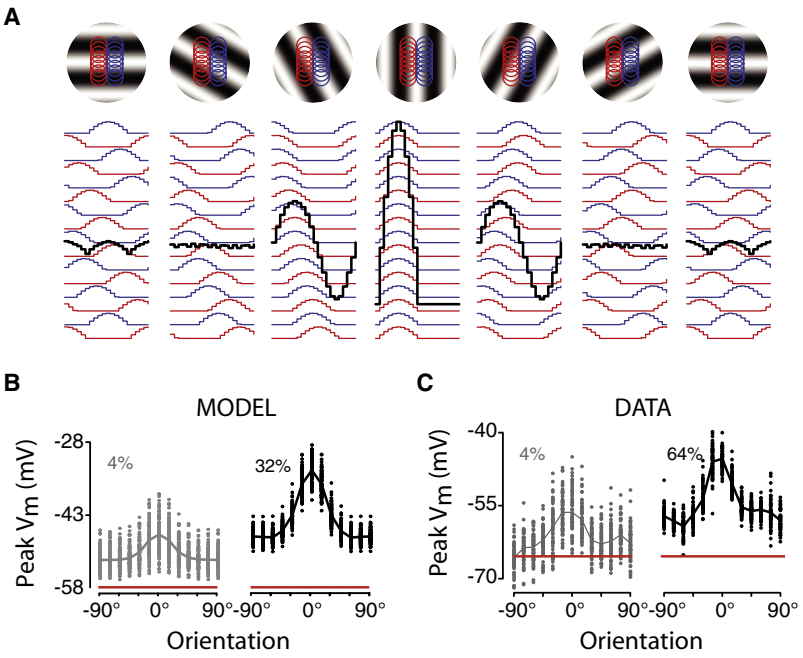

Figure 5. Feedforward Model of the Thalamocortical Circuit Incorporating LGN Variability and Correlations

(A) Mean responses of an array of 16 LGN neurons (red, ON; blue, OFF) to drifting gratings at different orientations. Black lines are mean V_m responses of a model simple cell that receives inputs from these 16 LGN neurons.

(B) Trial-to-trial the amplitude of the V_m response evoked in the model simple cell at low (left) and high (right) contrast and different orientation. Each dot is the peak V_m response evoked by one cycle of a drifting grating. Red lines correspond to resting potential of the model simple cell.

(C) Actual data of trial-to-trial V_m responses from intracellular recordings in an example simple cell, reproduced from Finn et al. (2007) for comparison with the model.

See also Figure S5.

evoke an increase in conductance of ~6 nS, which reduces the input resistance to 55 MΩ. This conductance increase is in the range of previous observations from cortical intracellular recordings (Monier et al., 2003; Anderson et al., 2000; Berman et al., 1991). Synaptic efficacy was modulated by short-term synaptic depression, modeled after Boudreau and Ferster (2005) (Equation 5 and Experimental Procedures).

Mean V_m responses at high-contrast for one iteration of the model are overlaid (black lines) on the mean responses of the 16 LGN inputs in Figure 5A (red, ON-center; blue, OFF-center). Single-cycle and mean response amplitudes as a function of orientation at low and high contrasts closely matched actual data recorded intracellularly from a simple cell (Figures 5B and 5C, data in C reproduced from Finn et al., 2007). The model qualitatively matched many features of the data, such as orientation tuning width, the extent of the trial-to-trial V_m variability, the relative orientation independence of trial-to-trial variability and the dependence of trial-to-trial variability on contrast.

To explore the range of the model's behavior, we simulated the responses of 50 simple cells, each receiving 16 LGN inputs whose properties were drawn from a different subset of recorded LGN cells. We measured the V_m response variability as trial-to-trial SD at the peak of the depolarization, and plotted variability at high contrast against variability at low contrast for preferred and null stimuli (Figures 6A and 6B, black) for each of the 50 model cells. For comparison, a similar measure of variability is plotted for 52 intracellularly recorded simple cells (orange points; from Finn et al., 2007). On average, V_m variability at 4% contrast was higher than the variability at 32% contrast, both for preferred and null stimuli in both the model and data (model: 42% higher for preferred, 23% higher for null; data: 51% higher for preferred, 30% higher for null). Variability for low-contrast preferred stimuli and high-contrast null stimuli are compared in Figure 6C. The former was 120% higher, matching the trend in intracellular data (not shown). These results were obtained with 4% as the low contrast. Similar values were obtained with 2% as the low contrast (48% higher for preferred, 28% higher for null, and 128% for low-contrast preferred against high-contrast null). The key criterion for contrast-invariance to occur, that low-contrast preferred variability be higher than high-contrast null variability, is therefore met by this model.

The Effect of the Model's Parameters on V_m Variability

The model—and the LGN data on which is it based – has a number of different features and parameters: the convergence of LGN input, the spatial organization of the LGN receptive fields, trial-to-trial variability in the LGN responses, cell-to-cell correlation in the variability, contrast dependence of LGN response mean, variability and correlation, synaptic depression, and finally the nonlinear transformation of synaptic conductance into changes in V_m. We now ask which of these features of the model and LGN data were critical in matching the model's behavior to the in vivo behavior recorded directly from simple cells. To do so we modified each aspect of the model in turn.

Neither the number of LGN inputs in the model nor the receptive field aspect ratio had a significant effect on the contrast sensitivity of V_m SD. To quantify this effect, we calculated the percent increase in V_m SD between high and low contrast for three different stimulus pairs: high and low contrast—preferred orientation, high and low contrast—null orientation, and high contrast—null and low contrast—preferred. For each of the three stimulus pairs, we explored three different receptive field aspect ratios (2:1, 3:1, and 4:1). Percent increase in V_m SD between high and low contrast for all nine conditions are plotted against number of LGN inputs in Figure S5A; little substantive change occurs when either the number of inputs or the subfield aspect ratio changes. The number of LGN inputs did have a small effect on the actual value of the V_m SD for all stimulus conditions (Figure S5B). As more LGN inputs are pooled, V_m SD decreases, by about 20% between 8 and 40 inputs.

Contrast-dependent changes in LGN response variability were, not surprisingly, essential to obtain contrast-dependent

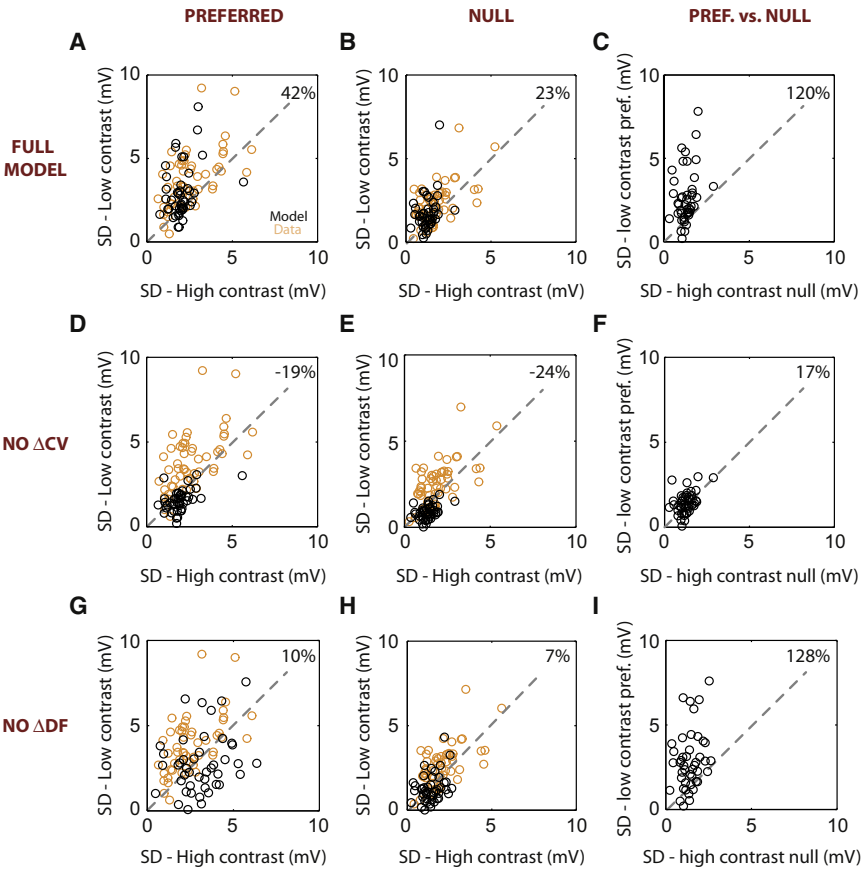

Figure 6. Contrast Dependence of Vm Variability in a Feedforward Model

(A and B) Model V_m SDs (black) at low contrast (4%) plotted against model V_m SDs at high contrast (32%) for gratings at the preferred orientation (A) and null orientation (B). Actual data from intracellular recordings in simple cells, from Finn et al. (2007) is also plotted for comparison (orange).

(C) Model V_m SDs for low-contrast preferred stimuli plotted against model Vm SDs for high-contrast null stimuli.

(D–F) Same as (A–C), but after removing the contrast-dependence of trial-to-trial variability from simulated LGN responses (black). Intracellular data (orange) is repeated from (A) and (B).

(G–I) Same as (A–C) but after replacing nonlinear summation in model simple cells by a comparably scaled linear transformation between total LGN input and simple cell V_m (black).

Intracellular data (orange) is repeated from (A) and (B). See also Figure S5.

V_m variability in V1. In simulations in which the variability of LGN responses was held constant across contrasts, the contrast dependence of V_m variability in the simple cell's V_m responses was abolished (compare Figures 6D–6F, orange and black). Pairwise correlation was (also not surprisingly) required for the model to generate sufficient levels of variability in the model simple cell's responses. V_m SD for three different stimulus conditions is plotted as a function of simulated pairwise correlation between the LGN inputs in Figure S5C. At the correlation level measured in the LGN data (vertical dashed line, r = 0.25), the average values of peak V_m SDs for the model were comparable to those obtained from intracellular recordings (1.32 mV versus 2.0 mV, 2.02 mV versus 2.6 mV, and 2.63 mV versus 3.8 mV for high-contrast null, high-contrast preferred, and low-contrast preferred stimuli). Changes in pairwise correlations between LGN inputs did not affect the increase in low-contrast preferred variability relative to high-contrast null variability: across all simulated values of pairwise correlations ranging from 0.05 to 0.70, low-contrast preferred variability was ~120% more than high-contrast null variability (orange line in Figure S5C).

For any excitatory synapse, the reversal potential (near 0 mV) dictates that a given increase in conductance starting from rest generates a much larger depolarization than the same increase starting from a high baseline of synaptic input. We explored the effect of this saturating nonlinearity simply by removing it from model. In Figures 6G–6I, for example, where the relationship between LGN activity and V_m is assumed to be linear, the difference between low- and high-contrast V_m variability almost completely disappears, both at the preferred (G) and null orientations (H). Low-contrast preferred stimuli, however, still evoked responses that were more variable than high-contrast null stimuli (I). The net effect of removing the conductance nonlinearity, then, is to remove the orientation-independence of V_m variability.

Synaptic depression introduces a similar saturating relationship between the firing rate of LGN inputs and V1 membrane potential. Unlike the conductance nonlinearity, however, when synaptic depression was removed from the model, only minor changes in V_m variability were observed (not shown)—compared to high-contrast stimuli, V_m SDs were 34% and 16% greater for preferred and null stimuli, and 88% greater for preferred low-contrast stimuli compared to null high-contrast stimuli.

How these parameters interact in the model is diagrammed in Figure 7. Here again we highlight the responses at low and high contrast and preferred and null orientation (shaded rectangles in Figures 7B, 7D, 7F, and 7H). The first step of the model is to calculate the mean conductance change originating from the LGN, and its trial-to-trial variability, after taking the modulation of synaptic efficacy by synaptic depression into account. These are plotted (curves and error bars) for high and low contrast in Figures 7B and 7F, the curves showing the mean conductance change, and error bars showing variability. The difference between variability at high and low contrast that occurs across all orientations arises from the contrast dependent changes in variability in the LGN inputs (CV). As described above, the correlation between LGN inputs is necessary for this variability to appear in simple cells despite the pooling of multiple inputs at the simple cell membrane.

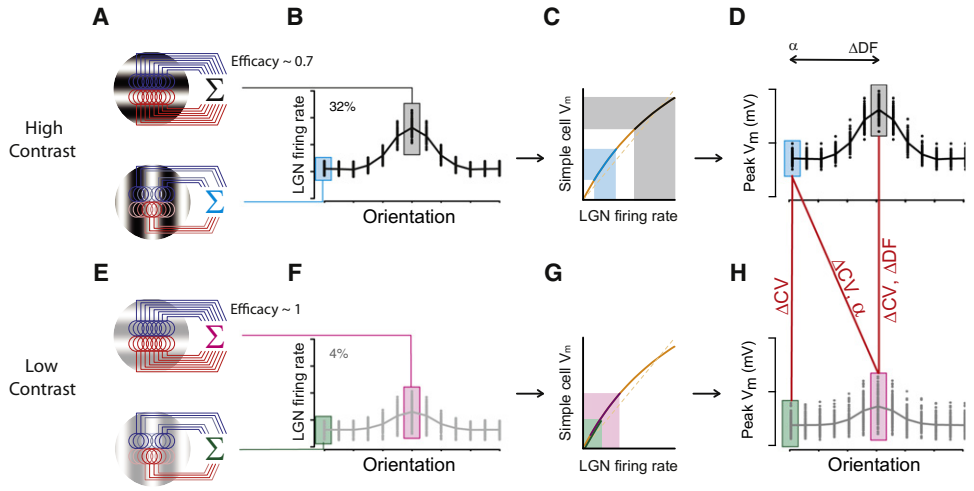

Figure 7. How Orientation-Independent, Contrast-Dependent V_m Variability Arises in Simple Cells

(A) Schematic of LGN neurons responding to gratings in the "preferred" or "null" orientations. Red and blue circles are receptive field centers of ON and OFF LGN neurons. Lines correspond to neurons responding to the stimulus, line color intensity corresponds to response strength. "Efficacy" denotes the modulation of synaptic strength at each contrast by short-term synaptic depression.

(B) Peak amplitude of the summed LGN responses for 100 trials (cycles) at each stimulus orientation, plotted as a function of orientation. Total LGN input to V1 at the preferred orientation is higher on average and has higher trial-to-trial variability than the null orientation (cyan shading) simply because more LGN cells are activated simultaneously by the preferred stimulus.

(C) In the model, the summed LGN responses generate a proportional change in conductance in the postsynaptic simple cells. The transformation of total LGN input to V_m therefore contains a compressive nonlinearity arising as a result of the reduced driving force on synaptic currents at large depolarizations (curved line). Because of the compressive nonlinearity, the trial-to-trial variability in V_m responses are comparable at preferred and null orientations. That is, the vertical extent of the cyan and gray shading where they meet the vertical axis (V_m variability at preferred and null orientations) are comparable, even though they differ in horizontal extent where they meet the horizontal axis (LGN input variability at preferred and null orientations).

(D) Peak amplitude of the simple cell V_m for 100 stimulus trials at each stimulus orientation, plotted as a function of stimulus orientation. Responses to high-contrast preferred (gray shading) and high-contrast null (cyan shading) are highlighted. V_m variability is relatively orientation independent because of the complementary effects of the aspect ratio (α) at null orientation and nonlinear summation at the preferred orientation (ΔDF).

(E–H) Same as (A)–(D) but for low-contrast stimuli. Shadings correspond to low-contrast preferred (magenta) and low-contrast null (green) stimuli.

See also Figure S5.

Unlike the variability in V_m of both the model and data (Figures 5B and 5C), the variability in the modeled synaptic input from the LGN (conductance, *g*) is strongly orientation dependent (Figures 7B and 7F). This dependence is a function of the elongation of the subfields, and that larger numbers of LGN afferents are activated simultaneously by the preferred stimulus compared to the null stimulus. As discussed above, the orientation dependent variability in *g* is transformed into the orientation independent variability in V_m by the saturating nonlinear relationship between *g* and V_m; removing the nonlinearity increases the orientation dependence of V_m variability (Figures 6G–6I). The mechanism underlying this transformation is illustrated in Figure 7C. The variability in *g* at the preferred orientation (gray) is higher than at the null orientation (cyan). Because that variability is occurring around a high mean *g* (Figure 7C, gray)—where the slope of the *g*-V_m curve is flatter—it gives rise to a comparable level of variability in V_m as does the variability in *g* at the null orientation, which varies around the much lower resting *g* (Figure 7C, cyan). The same compressive effect occurs, to a lesser degree, at low contrast (Figures 7F and 7G, magenta and green). As a result, the variability in V_m is less dependent on orientation (Figures 7D and 7G) than the variability in visually evoked conductance. Note that a more-rapidly saturating relationship between LGN activity and V_m could potentially make the variability more equal across orientations.

DISCUSSION

Historically, the feedforward model of visual cortex has been rightfully questioned for its failure to account for a large number of the response properties of simple cells: the sharpness of orientation tuning and its mismatch with receptive field maps, contrast invariance of orientation tuning and contrast-set gain control, cross-orientation suppression, contrast dependence of response phase, contrast dependence of preferred temporal frequency, and direction selectivity. All of these properties can be accounted for in models that incorporate cross-orientation inhibition or orientation-independent inhibition (Heeger, 1992; Troyer et al., 1998; Kayser et al., 2001; Lauritzen et al., 2001; Martinez et al., 2002; Lauritzen and Miller, 2003; Hirsch et al., 2003). In gain-control models, almost all of these properties emerge from a single underlying mechanism: a large shunting inhibition that is contrast dependent and orientation independent (Heeger, 1992; Carandini and Heeger, 1994; Carandini et al., 1997). The resulting change in input conductance accounts for contrast-dependent scaling of responses; the change in

membrane time constant accounts for the changes in response timing and preferred temporal frequency. Experimental evidence is equivocal, however, for the large, orientation independent conductance changes (up to 5X) required by the contrast gain control model (Ferster, 1986; Douglas et al., 1988; Berman et al., 1991; Borg-Graham et al., 1998; Anderson et al., 2000; Martinez et al., 2002; Monier et al., 2003).

As an alternative to inhibition-based models, we have asked whether the feedforward model can in fact account for most of the properties of simple cells when properties of thalamic neurons and thalamocortical synapses are incorporated (see Priebe and Ferster, 2008). These properties include significant nonlinear elements such as synaptic depression (e.g., Boudreau and Ferster, 2005), contrast saturation in thalamic neurons (e.g., Priebe and Ferster, 2006), spike threshold (e.g., Priebe et al., 2004), nonlinear summation of synaptic inputs, and more recently, contrast dependent changes in response variability (Anderson et al., 2000; Finn et al., 2007). Contrast dependent changes in response variability, however, could theoretically arise from within the cortical circuit (Monier et al., 2003; Sit et al., 2009; Rajan et al., 2010). We now show that contrast dependent response variability is also intrinsic to the feedforward pathway. Inactivating the cortical circuit has no significant effect on variability or its contrast dependence. And thalamic response variability, its dependence on contrast, and its cell-to-cell correlation can account for variability in the V_m responses of simple cells when applied to a feedforward model. All of these properties of the feedforward pathway can be measured experimentally, which makes for a highly constrained model with few free parameters.

The interactions among the different elements of the model are surprisingly complex. At every orientation and contrast, correlation in the variability of LGN neurons is critical for allowing that variability to appear in the simple cell. Other elements of the model come in to play in specific regions of the stimulus parameter space. Changes in orientation change the number of simultaneously active LGN neurons, which in turn changes the relationship between pre- and postsynaptic variability. Changes in stimulus contrast change the variability of individual LGN neurons. For stimuli that evoked large mean response amplitude, specifically, high contrasts and preferred orientations, the compressive nonlinearity of summation of synaptic inputs reduces response variability. And yet these diverse effects blend together to create a relationship between stimulus and response that can be summarized in the very simple mathematical terms of contrast gain control.

An earlier study of neurons in primate V1 suggested that spiking responses to briefly flashed gratings were not contrast invariant (Nowak and Barone, 2009). In that study, large stimuli (up to 9 times the receptive field size) at different spatial phases were used, and both simple and complex cells were pooled for analysis. In our study, however, we targeted only simple cells that likely received a large fraction of thalamic inputs, and we used smaller stimuli (comparable to receptive field size) at the optimal spatial phase at each orientation. These differences in experimental methodology might explain why we were able to observe contrast-invariant tuning in our data for flashed gratings.

Previous studies of response variability in LGN neurons have reported a wide range of behaviors, from sub-Poisson variability, with Fano factors as low as 0.32 (Gur et al., 1997; Kara et al., 2000; Reinagel and Reid, 2000; Liu et al., 2001), to supra-Poisson variability, with Fano factors as high as 1.5 (Levine and Troy, 1986; Levine et al., 1996; Reich et al., 1997; Hartveit and Heggelund, 1994; Sestokas and Lehmkuhle, 1988; Oram et al., 1999). Some of this large range is clearly a function of the stimulus contrast used (Hartveit and Heggelund, 1994; Sestokas and Lehmkuhle, 1988; Oram et al., 1999; see also Figure 3 above). In addition, different studies were based on different types of stimuli, such as drifting gratings, sparse noise, or flashing gratings. Finally, there were differences in preparation, ranging from awake primates to cats anesthetized with different agents. Given this range of results, what is critical for this study is that the LGN data on which the model is based were collected under precisely the same conditions as the intracellular cortical data to which the model was compared.

The model can be further elaborated by adding additional features, albeit at the expense adding free parameters. First, Gabor-shaped receptive fields could be used instead of rectangular receptive fields. This change would require more input neurons to match the variability observed in data because of the decrease in the efficacy of inputs at the edges of the receptive field. Second, the correlation between different pairs of LGN inputs could be allowed to vary (here, all pairwise correlations for a given model cell were identical). Third, the correlation could be allowed to vary as a function of orientation, and therefore of relative response phase. Fourth, in order to demonstrate that a purely feedforward circuit can accomplish contrast invariance, the model currently assumes that all of the input to a simple cell originates in the thalamus, whereas our data suggests that only ~50% of simple-cell inputs, on average, arise in the thalamus. Therefore, a cortical input source, along with the dependence of cortical variability and correlations on stimulus contrast (for example, Kohn and Smith, 2005) could also be included in the model. Each of these additions would alter the quantitative estimates that emerge from the model, such as the number of LGN inputs, the correlation level required to match variability in the cortical data, absolute values of V1 variability and magnitude of contrast-dependent changes in V_m noise. But the basic principles of the model, including the requirement for LGN variability and correlations, receptive field elongation, and a compressive nonlinearity in the transformation between LGN activity and V_m will likely still apply.

In the same way that LGN variability propagates to the cortex, variability in retinal ganglion cells might propagate to the LGN: retinal response variability is contrast dependent (Berry et al., 1997) and correlated between nearby cells (Meister et al., 1995). Variability in retinal ganglion cells, however, is much lower than that of LGN neurons (Levine and Troy, 1986; Levine et al., 1992, 1996; Kara et al., 2000). Some noise may therefore be introduced at the level of LGN by intrathalamic or feedback circuitry (Levine and Troy, 1986). These results, taken together with the strong synaptic connectivity between retinal ganglion cells and LGN neurons, suggest that a large portion of LGN variability and correlation may originate in the retina.

Although response variability is observed throughout the brain, we can suggest on the basis of our data that this variability may not need to be generated independently at each stage of processing. A large fraction of variability can be passed from area to area as long as sufficient correlations exist among the neurons in the input area. It should be emphasized, however, that the strength of the correlations need not be particularly high. A correlation of ~0.2 among LGN neurons was sufficient to explain the response variability in simple cells, and similar correlation levels (0.1–0.3) have been observed in spike responses of primate V1 (Kohn and Smith, 2005; Smith and Kohn, 2008; Gutnisky and Dragoi, 2008) and other cortical areas (Gawne et al., 1996; Cohen and Newsome, 2008; Cohen and Maunsell, 2009).

From previous work (Finn et al., 2007), it is known that weak (low contrast) preferred stimuli generate disproportionately large spike responses compared to strong (high contrast) null-oriented stimuli, even though they evoke similar mean depolarizations. This selective amplification is caused by the higher V_m variability for the former stimuli. We can now attribute that increase in variability to the combination of two factors: increase in variability at low stimulus strength in the thalamic inputs and an increase in the number of simultaneously active inputs for preferred stimuli. These factors seem generic: strong stimuli have been observed to reduce variability in a number of cortical areas (Churchland et al., 2010). It seems likely, then, that mechanisms similar to the ones we have identified here might operate throughout the neocortex.

EXPERIMENTAL PROCEDURES

Animal Preparation

Experiments were performed on anesthetized adult female cats aged 4–6 months. Anesthesia was induced with a ketamine-HCl (30 mg/kg i.m.)/acepromazine maleate (0.3 mg/kg i.m.) mixture and maintained by intravenous infusion of sodium thiopental (1–2 mg/kg/hr) or propofol (5–10 mg/kg/hr) and sufentanil (0.75–1.5 μg/kg/hr). Animals were paralyzed with pancuronium bromide (1.5 mg/kg induction, 0.2 mg/kg/hr maintenance) and artificially ventilated through a tracheal cannula to maintain end tidal CO_2 at 3.6%–4.0%). The thoracic vertebrae were suspended and a bilateral pneumothoracotomy was performed for recording stability. Core temperature was maintained at 37.8°C. Anesthetic depth was assessed by EEG and heart rate, and the anesthetic infusion rate was adjusted accordingly. All procedures were approved by the Northwestern University Animal Care and Use Committee.

Visual Stimulation

The nictitating membranes were retracted with 2.5% phenylephrine hydrochloride and pupils dilated with 1% atropine. Contact lenses and external corrective lenses focused the retina on a computer monitor (ViewSonic, Walnut, CA) ~48 cm distant (refresh rate 100 Hz; mean luminance 20 cd/m^2). Visual stimuli were generated with the Psychophysics Toolbox (Brainard, 1997; Pelli, 1997) for Matlab (Mathworks, Natick, MA). Sparse noise stimuli for receptive field mapping consisted of 0.5° × 0.5° pixels over an extent of 5° × 5°. Drifting grating stimuli (2 or 4 cycles/s) were presented at the optimal spatial frequency (0.3–1.2 cyc/deg), 13 orientations and 5 contrasts (2%–32%). For LGN recordings, grating size and position were set to overlap the receptive fields of all LGN neurons under study. For V1 recordings, high contrast (64%) gratings at optimal spatial frequency and size were used to determine preferred orientation and receptive field location. Flashed gratings at 5 phases were used to determined optimal phase at 6 different orientations (see Figure S1A). We presented flashed gratings at 6 orientations and 4 contrasts (4%– 32%) for 23 cells, and a shorter stimulus set (2 orientations 4 contrasts) for 12 cells.

Whole-Cell Recordings in V1

Whole-cell current clamp recordings were obtained with glass-electrodes (Sutter Instrument, Novato, CA) filled with standard K-gluconate solution with blind-patch techniques. Electrode impedance ranged from 7–12 MΩ. The pipette was positioned such that its tip, after ~600 μm travel through the cortex, was within 1 mm of the metal electrode used for cortical inactivation. Warm agarose (3%) was poured over the craniotomy to dampen cortical pulsations. Signals were low-pass filtered and digitized at 4,096 samples/s. For a cell to be included in the data set, we required that its resting potential at break-in be more hyperpolarized than −50 mV, and that the resting potential be stable over the course of the recording (Figure S1B).

Electrical Stimulation

Electrical stimuli (300–400 μA, electrode negative; 200 μs) were delivered to the cortex with low impedance (<2 MΩ) epoxy-coated tungsten electrodes (A-M Systems, Carlsborg, WA) placed at a distance of less than 1 mm from the patch pipette and ~400 μm below the cortical surface. Such stimulation creates a short window (~50–100 ms) during which cortical spiking activity is silenced (Chung and Ferster, 1998), but LGN activity is spared. Flashed grating stimuli (10 ms duration) were presented simultaneously with the shock.

Extracellular Recordings in LGN

Twenty-one groups of 2–4 simultaneous LGN unit recordings were obtained with two to four quartz-coated platinum-tungsten electrodes (impedance 1–3 MΩ) mounted on a 7-electrode microdrive (Thomas Recording GmBH, Giessen, Germany). A custom guide tube narrowed the spacing between electrodes to ~125 μm. Signals were band-pass filtered (300 Hz–5 kHz) and digitized at 10,000 samples/s. Spike sorting was performed offline with custom software written in Matlab, based on window discrimination followed by manual graphical cluster-cutting of the first three principal components of the spike waveform. We most often sorted only one spike per electrode, but in a few cases, a second spike waveform could be reliably discriminated. Recordings were from the A layers of the LGN and predominantly from X cells; 19 of 71 LGN neurons were OFF center.

Analysis

Analysis was performed offline with custom software written in Matlab. Spikes were detected and removed from the V_m traces by linear interpolation. The mean and SD of the V_m responses to flashing gratings were calculated from at least 15 repetitions of each stimulus condition, after smoothing the responses with a 5 ms boxcar filter. We defined the peak mean response as the highest mean response in an analysis window between 30 ms and 120 ms of stimulus onset. Peak V_m SD was calculated from a 2.5 ms window centered at the peak location. Baseline V_m SD was calculated in a 2.5 ms window, starting 5 ms after the onset of the visual stimulus or shock to avoid the influence of the shock artifact. For display, the shock artifact was removed by subtracting the shock-only trace (no visual stimulus presented). All parameters were measured without baseline subtraction. "Low-contrast," which refers to the lowest contrast for which we obtained a positive mean peak V_m response, was 4% (lowest contrast tested) for 23/35 cells and 8% for 12/35 cells. Tuning width was taken to be σ of a least-squares Gaussian fit to the average peak amplitudes with four free parameters: amplitude, preferred orientation, width, and offset.

In LGN recordings, each positive half-cycle of the drifting grating was treated as a separate trial. Spike counts were pooled across orientations for calculating response mean and variance as a function of contrast to obtain between 960 and 4,800 stimulus cycles for each contrast. Pairwise correlations between LGN neurons were calculated as the Pearson correlation coefficients of spike counts on a trial-to-trial basis (Kohn and Smith, 2005 and references therein). Since correlation between pairs of neurons depended on relative response phase, we also calculated pairwise correlations separately for in-phase responses, where the cycle post-stimulus time histograms (PSTHs) of the two neurons overlapped by more than

70% (by area), and for out-of-phase responses for which the overlap was less than 30%. The all-way shuffle predictor of the pairwise correlations (<0.01 in all cases) was calculated by randomly assigning trial identities 500 times and was subtracted from the reported correlation values. Fewer stimulus cycles were used to compute the correlations for the in-phase and out-of-phase cases due to the additional constraint of PSTH overlap (range: 400–960 trials).

Feedforward Model

Model simple cells were constructed to have two adjacent subfields, ON and OFF, each with an aspect ratio of 3 (Kara et al., 2002). Each subfield consisted of 8 LGN inputs with their receptive field centers distributed evenly along the axis of preferred orientation. For each stimulus contrast, each LGN input neuron was defined by its mean spike count per cycle (μ_{sc}) and coefficient of variation of spike count (CV, SD divided by mean). In our LGN recordings, the spread of variability within each recording group was much lower than the spread of variability pooled over the entire population of recorded cells. To better simulate groups of nearby LGN cells that all synapse onto a modeled simple cell, we always based the model's LGN inputs on neurons that were studied in a single recording session. To do so, for each instance of the model, we chose one LGN neuron and drew the mean counts and CV's of the 16 input neurons from a normal distribution, with means equal to that of the chosen neuron and variances computed from the variation of these parameters among neurons that were within the chosen neuron's recording group. For each stimulus condition, 100 stimulus cycles were presented to the model, with input spike counts determined by μ_{sc} and CV chosen for each input. This procedure was repeated for 50 iterations, with parameters drawn from different, randomly chosen subsets of the recorded LGN population.

To simulate pairwise correlations between LGN neurons, the total spike count variability in each LGN neuron was divided into two distinct parts, the "local" and "global" variability such that:

$$\sigma^2_{total} = \sigma^2_{local} + \sigma^2_{global}$$

$$\sigma^2_{global} = r^2 \sigma^2_{local} \quad \text{(Equation 3)}$$

where the local and global variances were related through the factor r. On each stimulus trial j, we determined the spike count of neuron i as

$$S^i_j = \eta^i_j + \xi_j \quad \text{(Equation 4)}$$

where η^i_j is a random number drawn from $N(\mu^i_{sc}, \sigma^2_{i,local})$ for each i and j, and ξ_j is a random number drawn from $N(0, \sigma^2_{global})$ for each j (identical for all i), with N being the normal distribution. Changing the value of r altered the relative weighting of local to global variability and thus varied the spike count correlation among the input neurons. We varied r such that correlations between input neurons varied between ~0.08 and ~0.68. These values were then interpolated linearly over the [0.05, 0.70] range in steps of 0.01. For computational simplicity, we assumed that sub-populations of input neurons would be simultaneously excited by drifting gratings at different orientations, and a single correlation value of 0.25, which corresponds to the mean correlation observed in our data for in-phase stimuli, was used unless otherwise stated.

LGN response PSTHs were modeled as half-wave rectified sinusoids, and scaled to the model cell's firing rate on each trial. The postsynaptic conductance change evoked by each LGN cell was modified by synaptic depression as measured experimentally (Boudreau and Ferster, 2005). Synaptic efficacy depended on input firing rate (computed in 12.5 ms bins), reaching an asymptote at 70% of the original value at high input rates:

$$Efficacy(t) = 0.7 + 0.3e^{-rate(t)/25} \quad \text{(Equation 5)}$$

Evoked conductance depressed to ~90%, ~75%, and ~70% of its nondepressed value at LGN firing rates of 20 Hz, 50 Hz, and 100 Hz. The summed input evoked a depolarization according to Equation 1 and Equation 2. The simple cell was modeled as a point neuron in steady-state, i.e., conductance changes were assumed to occur on a time scale slower than the membrane time constant. No active conductances or inhibitory inputs were included.

SUPPLEMENTAL INFORMATION

Supplemental Information includes five figures and can be found with this article online at doi:10.1016/j.neuron.2012.05.007.

ACKNOWLEDGMENTS

We are grateful to Dr. Kenneth D. Miller, Dr. Mark M. Churchland, and Dr. Nicholas J. Priebe for many insightful comments and suggestions on the manuscript and Jianing Yu and Hirofumi Ozeki for helpful discussions. This work was supported by NIH grant R01 EY04726 to D.F.

Accepted: May 5, 2012
Published: June 6, 2012

REFERENCES

Alitto, H.J., and Usrey, W.M. (2004). Influence of contrast on orientation and temporal frequency tuning in ferret primary visual cortex. J. Neurophysiol. *91*, 2797–2808.

Anderson, J.S., Carandini, M., and Ferster, D. (2000). Orientation tuning of input conductance, excitation, and inhibition in cat primary visual cortex. J. Neurophysiol. *84*, 909–926.

Berman, N.J., Douglas, R.J., Martin, K.A., and Whitteridge, D. (1991). Mechanisms of inhibition in cat visual cortex. J. Physiol. *440*, 697–722.

Berry, M.J., Warland, D.K., and Meister, M. (1997). The structure and precision of retinal spike trains. Proc. Natl. Acad. Sci. USA *94*, 5411–5416.

Borg-Graham, L.J., Monier, C., and Frégnac, Y. (1998). Visual input evokes transient and strong shunting inhibition in visual cortical neurons. Nature *393*, 369–373.

Boudreau, C.E., and Ferster, D. (2005). Short-term depression in thalamocortical synapses of cat primary visual cortex. J. Neurosci. *25*, 7179–7190.

Brainard, D.H. (1997). The Psychophysics Toolbox. Spat. Vis. *10*, 433–436.

Carandini, M., and Heeger, D.J. (1994). Summation and division by neurons in primate visual cortex. Science *264*, 1333–1336.

Carandini, M., Heeger, D.J., and Movshon, J.A. (1997). Linearity and normalization in simple cells of the macaque primary visual cortex. J. Neurosci. *17*, 8621–8644.

Chung, S., and Ferster, D. (1998). Strength and orientation tuning of the thalamic input to simple cells revealed by electrically evoked cortical suppression. Neuron *20*, 1177–1189.

Churchland, M.M., Yu, B.M., Cunningham, J.P., Sugrue, L.P., Cohen, M.R., Corrado, G.S., Newsome, W.T., Clark, A.M., Hosseini, P., Scott, B.B., et al. (2010). Stimulus onset quenches neural variability: a widespread cortical phenomenon. Nat. Neurosci. *13*, 369–378.

Cohen, M.R., and Maunsell, J.H. (2009). Attention improves performance primarily by reducing interneuronal correlations. Nat. Neurosci. *12*, 1594–1600.

Cohen, M.R., and Newsome, W.T. (2008). Context-dependent changes in functional circuitry in visual area MT. Neuron *60*, 162–173.

Douglas, R.J., Martin, K.A., and Whitteridge, D. (1988). Selective responses of visual cortical cells do not depend on shunting inhibition. Nature *332*, 642–644.

Ferster, D. (1986). Orientation selectivity of synaptic potentials in neurons of cat primary visual cortex. J. Neurosci. *6*, 1284–1301.

Ferster, D., and Miller, K.D. (2000). Neural mechanisms of orientation selectivity in the visual cortex. Annu. Rev. Neurosci. *23*, 441–471.

Finn, I.M., Priebe, N.J., and Ferster, D. (2007). The emergence of contrast-invariant orientation tuning in simple cells of cat visual cortex. Neuron *54*, 137–152.

Gawne, T.J., Kjaer, T.W., Hertz, J.A., and Richmond, B.J. (1996). Adjacent visual cortical complex cells share about 20% of their stimulus-related information. Cereb. Cortex *6*, 482–489.

Gur, M., Beylin, A., and Snodderly, D.M. (1997). Response variability of neurons in primary visual cortex (V1) of alert monkeys. J. Neurosci. *17*, 2914–2920.

Gutnisky, D.A., and Dragoi, V. (2008). Adaptive coding of visual information in neural populations. Nature *452*, 220–224.

Hartveit, E., and Heggelund, P. (1994). Response variability of single cells in the dorsal lateral geniculate nucleus of the cat. Comparison with retinal input and effect of brain stem stimulation. J. Neurophysiol. *72*, 1278–1289.

Heeger, D.J. (1992). Normalization of cell responses in cat striate cortex. Vis. Neurosci. *9*, 181–197.

Hirsch, J.A., Martinez, L.M., Pillai, C., Alonso, J.M., Wang, Q., and Sommer, F.T. (2003). Functionally distinct inhibitory neurons at the first stage of visual cortical processing. Nat. Neurosci. *6*, 1300–1308.

Hubel, D.H., and Wiesel, T.N. (1962). Receptive fields, binocular interaction and functional architecture in the cat's visual cortex. J. Physiol. *160*, 106–154.

Kara, P., Reinagel, P., and Reid, R.C. (2000). Low response variability in simultaneously recorded retinal, thalamic, and cortical neurons. Neuron *27*, 635–646.

Kara, P., Pezaris, J.S., Yurgenson, S., and Reid, R.C. (2002). The spatial receptive field of thalamic inputs to single cortical simple cells revealed by the interaction of visual and electrical stimulation. Proc. Natl. Acad. Sci. USA *99*, 16261–16266.

Kayser, A., Priebe, N.J., and Miller, K.D. (2001). Contrast-dependent nonlinearities arise locally in a model of contrast-invariant orientation tuning. J. Neurophysiol. *85*, 2130–2149.

Kohn, A., and Smith, M.A. (2005). Stimulus dependence of neuronal correlation in primary visual cortex of the macaque. J. Neurosci. *25*, 3661–3673.

Lauritzen, T.Z., and Miller, K.D. (2003). Different roles for simple-cell and complex-cell inhibition in V1. J. Neurosci. *23*, 10201–10213.

Lauritzen, T.Z., Krukowski, A.E., and Miller, K.D. (2001). Local correlation-based circuitry can account for responses to multi-grating stimuli in a model of cat V1. J. Neurophysiol. *86*, 1803–1815.

Levine, M.W., and Troy, J.B. (1986). The variability of the maintained discharge of cat dorsal lateral geniculate cells. J. Physiol. *375*, 339–359.

Levine, M.W., Cleland, B.G., and Zimmerman, R.P. (1992). Variability of responses of cat retinal ganglion cells. Vis. Neurosci. *8*, 277–279.

Levine, M.W., Cleland, B.G., Mukherjee, P., and Kaplan, E. (1996). Tailoring of variability in the lateral geniculate nucleus of the cat. Biol. Cybern. *75*, 219–227.

Liu, R.C., Tzonev, S., Rebrik, S., and Miller, K.D. (2001). Variability and information in a neural code of the cat lateral geniculate nucleus. J. Neurophysiol. *86*, 2789–2806.

Martinez, L.M., Alonso, J.M., Reid, R.C., and Hirsch, J.A. (2002). Laminar processing of stimulus orientation in cat visual cortex. J. Physiol. *540*, 321–333.

Meister, M., Lagnado, L., and Baylor, D.A. (1995). Concerted signaling by retinal ganglion cells. Science *270*, 1207–1210.

Monier, C., Chavane, F., Baudot, P., Graham, L.J., and Frégnac, Y. (2003). Orientation and direction selectivity of synaptic inputs in visual cortical neurons: a diversity of combinations produces spike tuning. Neuron *37*, 663–680.

Nowak, L.G., and Barone, P. (2009). Contrast adaptation contributes to contrast-invariance of orientation tuning of primate V1 cells. PLoS ONE *4*, e4781.

Oram, M.W., Wiener, M.C., Lestienne, R., and Richmond, B.J. (1999). Stochastic nature of precisely timed spike patterns in visual system neuronal responses. J. Neurophysiol. *81*, 3021–3033.

Pelli, D.G. (1997). The VideoToolbox software for visual psychophysics: transforming numbers into movies. Spat. Vis. *10*, 437–442.

Priebe, N.J., and Ferster, D. (2006). Mechanisms underlying cross-orientation suppression in cat visual cortex. Nat. Neurosci. *9*, 552–561.

Priebe, N.J., and Ferster, D. (2008). Inhibition, spike threshold, and stimulus selectivity in primary visual cortex. Neuron *57*, 482–497.

Priebe, N.J., Mechler, F., Carandini, M., and Ferster, D. (2004). The contribution of spike threshold to the dichotomy of cortical simple and complex cells. Nat. Neurosci. *7*, 1113–1122.

Rajan, K., Abbott, L.F., and Sompolinsky, H. (2010). Stimulus-dependent suppression of chaos in recurrent neural networks. Phys. Rev. E Stat. Nonlin. Soft Matter Physiol. *82*, 011903.

Reich, D.S., Victor, J.D., Knight, B.W., Ozaki, T., and Kaplan, E. (1997). Response variability and timing precision of neuronal spike trains in vivo. J. Neurophysiol. *77*, 2836–2841.

Reinagel, P., and Reid, R.C. (2000). Temporal coding of visual information in the thalamus. J. Neurosci. *20*, 5392–5400.

Sclar, G., and Freeman, R.D. (1982). Orientation selectivity in the cat's striate cortex is invariant with stimulus contrast. Exp. Brain Res. *46*, 457–461.

Sestokas, A.K., and Lehmkuhle, S. (1988). Response variability of X- and Y-cells in the dorsal lateral geniculate nucleus of the cat. J. Neurophysiol. *59*, 317–325.

Sit, Y.F., Chen, Y., Geisler, W.S., Miikkulainen, R., and Seidemann, E. (2009). Complex dynamics of V1 population responses explained by a simple gain-control model. Neuron *64*, 943–956.

Skottun, B.C., Bradley, A., Sclar, G., Ohzawa, I., and Freeman, R.D. (1987). The effects of contrast on visual orientation and spatial frequency discrimination: a comparison of single cells and behavior. J. Neurophysiol. *57*, 773–786.

Smith, M.A., and Kohn, A. (2008). Spatial and temporal scales of neuronal correlation in primary visual cortex. J. Neurosci. *28*, 12591–12603.

Troyer, T.W., Krukowski, A.E., Priebe, N.J., and Miller, K.D. (1998). Contrast-invariant orientation tuning in cat visual cortex: thalamocortical input tuning and correlation-based intracortical connectivity. J. Neurosci. *18*, 5908–5927.